J Mater Sci (2008) 43:5837–5844
DOI 10.1007/s10853-008-2847-z

Role of structure and morphology in the elastic modulus of carbon nanotube composites

Shiren Wang

Received: 10 July 2007 / Accepted: 30 June 2008 / Published online: 31 July 2008

Abstract The nature of nanoscale reinforcements in the carbon nanotube composites indicates nanocomposite properties are heavily dependent on the micro/nano-structure and morphology. Macroscopic parameter-based properties estimation may lead to deviation as large as 30%. In this paper, a modified shear-lag model, combined with probability statistical theory and composites morphology, is established to investigate the elastic properties of single wall carbon nanotubes (SWNTs)-reinforced polymer composites. The computational results indicated that elastic modulus of nanocomposite was remarkably dependent on the micro/nano-structure, including diameter, length, and orientation of the dispersed SWNTs. Microstructure-dependent shape factor and orientation effect factor played a key role on achieving high-performance nanocomposites. Elastic modulus of nanocomposite with well-dispersed carbon nanotubes was more susceptible to the orientation. Similarly, nanocomposite modulus was more subject to the dispersion influence when SWNTs were well-aligned. The maximal modulus was located in the zone of small rope diameters and small orientation angles when adequate interfacial bonding was provided. The computational results were also compared with experimental outcome and demonstrated good consistence.

S. Wang (✉)
Department of Industrial Engineering, Texas Tech University, Lubbock, TX 79409, USA
e-mail: Shiren.Wang@ttu.edu

Introduction

Since the discovery of carbon nanotubes (CNTs), it has been investigated in a variety of fields including chemistry, physics, material science, and electronics. CNTs are molecular-scale tubes of graphitic carbon with outstanding properties, such as exceptional elastic modulus, tensile strength, unique thermal conductivity, and electrical conductivity [1, 2]. Carbon nanotubes are the strongest fibers that are currently known. The Young's Modulus of single-walled carbon nanotubes (SWNTs) has been calculated to $\sim$1 TPa by taking wall thickness as 0.34 nm [3]. Due to van der Waals interactions, SWNTs usually self-assemble into SWNT ropes. The Young's modulus of SWNT rope composed of $\sim$1 nm diameter individual tubes have been experimentally measured in the range of 600–700 GPa [4, 5]. The tensile strength of individual SWNT was theoretically estimated to be $\sim$200 GPa [6], while experimental measurement indicated that it was $\sim$50 GPa [7–9] for a SWNT rope composed of several individual tubes with 1 nm diameter. Beside their well-known extra-high mechanical properties, SWNTs offer either metallic or semiconductor characteristics based on the chiral structure of fullerene [10]. They also possess superior thermal and electrical properties. For example, thermal conductivity is about twice as high as diamond, and electric current carrying capacity is $\sim$1000 times greater than copper wire [11]. These unique properties have inspired interest in using CNTs as reinforcement in polymer composites to acquire ultra-light structure materials with multifunctional features, such as desired electromagnetic interference, flame-retardant performance, or enhanced electrical conductivity. SWNTs are regarded as the most promising reinforcement material for the next generation of high-performance structural and multifunctional composites.

If the exceptional properties of SWNT could be effectively incorporated into a polymer matrix, nanocomposites can be achieved with lightweight and exceptional strength and stiffness. The effective utilization of nanotubes for composites applications depends on the ability to disperse the nanotubes uniformly throughout the matrix. Carbon nanotubes are anisotropic in nature. Therefore, it is very important to take advantage of the nanotubes in the axial direction, controlled tube orientation, or degree of alignment of nanotubes in the polymer matrix in order to realize their exceptional mechanical and functional properties. In addition, the smooth surface of CNTs also reduces the load-transfer capacity and diminishes the nanocomposites properties. Functionalization of CNTs is regarded as one of the effective methods to improve the load-transfer so that high-performance nanocomposites can be achieved. Accurate models of how these issues influence the effective properties of the SWNTs-reinforced polymer will be necessary to optimize the fabrication and effective properties of SWNTs polymer systems. A great deal of research has addressed the effects of orientation and aspect ratio of short fibers on the overall elastic moduli of composites, especially for the composites with aligned fibers and random-oriented fibers. These methods include the dilute model based on Eshelby's equivalent inclusion [12–14], the self-consistent model for finite-length fibers [15–17], the Mori–Tanaka's model [18–21], the Halpin–Tsai equation and its extensions [22, 23], recent micromechanical model [24], and Finite element based model [25]. However, most of previous models simply take average diameter and length of fibers to estimate the overall elastic moduli. The simplifications in the prediction may lead to large deviation, some times, more than 30% [26]. The classical shear-lag model originated by Cox [27] was later elucidated by Nayfeh [28], McCartney [29], and Nairn [30] in the context of linear elasticity. Fukuda and kawaka [31] proposed a simple model to estimate the composite elastics based on the shear-lag theory. Jayaraman and Kortschot [32] have found that there was a mistake in the calculation of the force sustained by the fibers across the scan line in the derivations of Fukuda and Kawaka. The average load-direction component of the axial force is found by averaging over all the fibers in the specimen rather than averaging over the fibers that cross the scan line. The magnitude of the error depends on the fiber orientation distribution, length distribution, and the magnitude of the shear-lag effect. Kallmes et al. [33] also investigated shear-lag theory and used a paper physical approach (PPA) to estimate the elastic modulus. It was found that the modulus contribution from fibers would be negative by using PPA method when orientation angle was larger than $\theta = \arcsin [1/(1 + v_{12})]^{1/2}$, since the orientation factor was calculated to be negative in this situation [16]. However, the off-axis modulus of fibers should always be positive whatever the orientation angle is [31]. Particularly, in the case of the fiber orientation angle between the fiber-axis direction and the applied strain direction being comparatively large, the PPA method would be invalid in the predicting the elastic modulus of composite. The experimental results [34] also validated that the theoretical results predicted by PPA are lower than the corresponding experiment data. The reasons stem from the imprecise calculation for the off-axis stress and possible negative value for the orientation factor in the large orientation angle.

In this paper, the improved shear-lag model is further modified for elastic modulus prediction by considering both probability statistics theory and micro/nano-structure of the nanocomposites. The influence of microstructure-dependent shape factor and orientation factor on elastic properties is further elucidated.

Theoretic modeling

For carbon nanotubes-reinforced nanocomposites, a carbon nanotube with radius r is encased in a concentric cylindrical shell of matrix having radius R (Fig. 1).

The axial strain ε_{zz} and shear strain γ_{rz} are given in the terms of the displacement:

$$\varepsilon_{zz} = \frac{\partial w}{\partial z} \tag{1}$$

$$\gamma_{rz} = \frac{\partial u}{\partial z} + \frac{\partial w}{\partial r} \tag{2}$$

where u, w are the displacement in the z and r directions.

The strain in the axial direction can be given according to the constitutive equations:

$$\varepsilon_{zz} = \frac{1}{E_1}(\sigma_{zz} - v(\sigma_{rz} + \sigma_{\theta\theta})) \tag{3}$$

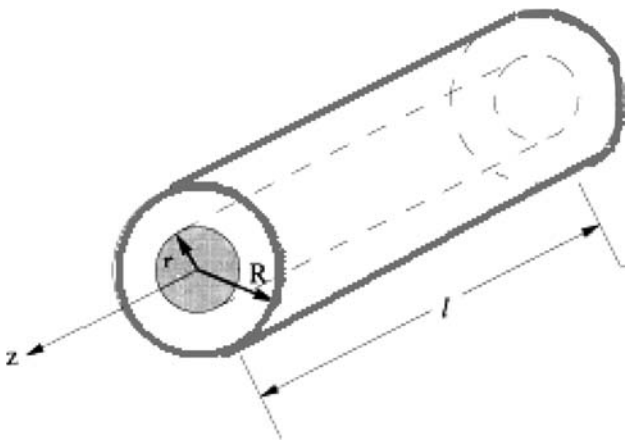

Fig. 1 A single carbon nanotube encased in the polymer matrix [27]

where σ_{zz} and σ_{rz} are axial and radial direction stress, respectively. $\sigma_{\theta\theta}$ is the stress in the direction perpendicular to the planes of σ_{zz} and σ_{rz}.

G_1, G_2 represent the shear modulus; E_1, E_2 denote the Young's modulus; v_1, v_2 denote the Poisson ratio in the two main stress directions. The governing equations for axismmetric problem, in a displacement formulation and in terms of axis equilibrium, are given in the following equations:

$$\frac{\partial \tau_{rz}}{\partial r} + \frac{\partial \sigma_{zz}}{\partial z} + \frac{\tau_{rz}}{r} = 0 \tag{4}$$

$$\frac{\partial \sigma_{rr}}{\partial r} + \frac{\partial \tau_{rz}}{\partial z} + \frac{\sigma_{rr} - \sigma_{\theta\theta}}{r} = 0 \tag{5}$$

where

$$\sigma_{zz} = \frac{\partial}{\partial r}\left(c\frac{\partial^2 \Psi}{\partial r^2} + \frac{c}{r}\frac{\partial \Psi}{\partial r} + d\frac{\partial^2 \Psi}{\partial z^2}\right) \tag{6}$$

$$\tau_{rz} = \frac{\partial}{\partial r}\left(\frac{\partial^2 \Psi}{\partial r^2} + \frac{1}{r}\frac{\partial \Psi}{\partial r} + a\frac{\partial^2 \Psi}{\partial z^2}\right) \tag{7}$$

$$u = \frac{b-1}{2G_2}\frac{\partial^2 \Psi}{\partial r \partial z} \tag{8}$$

The parameters of a, b, c, and d are defined as follows:

$$a = \frac{-v_1(1+v_2)}{1-\frac{v_1^2 E_2}{E_1}} \tag{9}$$

$$b = \frac{v_2 - \frac{v_1 E_2}{E_1}\left(\frac{E_1}{G_1} - v_1\right)}{1-\frac{v_1^2 E_2}{E_1}} \tag{10}$$

$$c = \frac{\frac{E_1}{G_1} - v_1(1+v_2)}{1-\frac{v_1^2 E_2}{E_1}} \tag{11}$$

$$d = \frac{\frac{E_1}{2G_2}(1-v_2)}{1-\frac{v_1^2 E_2}{E_1}} \tag{12}$$

The stress function was given by [30]:

$$\Psi = f(z) + g_1(r)z + g_2(r) \tag{13}$$

where $f(z)$ is a function only of z and $g_1(r)$, $g_2(r)$ are functions only of r.

A common solution is given as follows [30]:

$$\frac{\partial^2 \sigma_f}{\partial z^2} - \beta^2 \sigma_f = \text{constant} \tag{14}$$

where σ_f is the tensile strength of the fiber and β is the parameter related to the materials properties. For the far away from stress transfer zone, the fiber axial stress will settle into the far-field stress, σ_f, and the derivative term will be zero [30]. The constant must therefore be $-\beta^2\sigma_f$. The final equation, which is identical to Cox's (1952) equation, is

$$\frac{\partial^2 \sigma_f}{\partial z^2} - \beta^2 \sigma_f = -\beta^2 \sigma_{f\infty} \tag{15}$$

But the definition of β previously defined by Cox is different

$$\beta^2 = \frac{2}{r^2 E_f E_m}\left[\frac{E_f V_1 + E_m V_2}{\frac{V_2}{4G^f} + \frac{1}{2G^m}\left(\frac{1}{V_2}\ln\left(\frac{1}{V_1}\right) - 1 - \frac{V_2}{2}\right)}\right] \tag{16}$$

where E_f, E_m indicate the Young's modulus of fiber and matrix; V_1, V_2 represent the volume percentage of fiber and matrix; G^f, G^m denote the shear modulus of fiber and matrix.

The Poisson ratio can also be derived by the following equations:

$$v_1 = \frac{r^2}{R^2}, \qquad v_2 = \frac{R^2 - r^2}{R^2} \tag{17}$$

Solving the Eq. 15 resulted in Eq. 18:

$$\bar{\sigma}_f = E_f \bar{\varepsilon}_0\left[1 - \frac{\tanh(\beta l/2)}{\beta l/2}\right] \tag{18}$$

$\bar{\sigma}_f$ is the average tensile strength of the fiber, and $\bar{\varepsilon}_0$ is the average strain. E_f is the Young's modulus of the fiber and l is the fiber length.

Assume the following formulation:

$$\eta_L = 1 - \frac{\tanh(\beta l/2)}{\beta l/2} \tag{19}$$

Let A_f denote the cross-section area of fiber, then the load of the fiber in longitude direction can be formulated as:

$$F = E_f \bar{\varepsilon}_0 A_f \eta_L \tag{20}$$

To redefine the shape factor and orientation factor, a single misaligned fiber was considered. Similar to the calculation of axis load, for a misaligned short-fiber with an angle θ between the referred x direction and fiber axis direction, the applied force in the x-direction on this individual fiber can be calculated as follows (Fig. 2):

$$F_x = E_x \varepsilon_x \eta_L (A_f \cos\theta) \tag{21}$$

E_x is the off-axis, A_f is the cross-section area of the tube. On the other hand, off-axis modulus E_x can be computed as follows [33]:

$$\frac{1}{E_x} = \frac{1}{E_1}(\cos^4\theta) + \frac{1}{E_2}(\sin^4\theta) + \left(\frac{1}{G_{12}} - \frac{2v_{12}}{E_1}\right)\sin^2\theta\cos^2\theta \tag{22}$$

E_1, E_2 are the Young's modulus in longitudinal and transverse directions, respectively. G_{12} is the shear modulus and v_{12} is the in-plane Poisson ration. θ is the orientation angle.

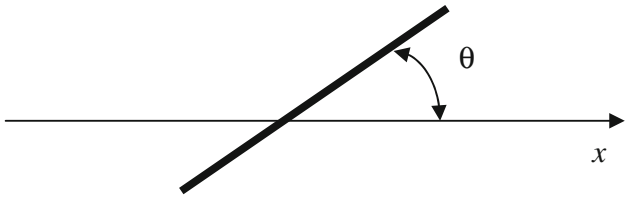

Fig. 2 A single misaligned carbon nanotubes aligned [32]

Re-organizing Eq. 22 resulted in the solution of the off-axis modulus:

$$E_x = \frac{E_1 E_2}{E_2 \cos^2\theta\left(\cos^2\theta + \left(\frac{E_1}{G_{12}} - 2v_{12}\right)\sin^2\theta\right) + E_1 \sin^4\theta} \tag{23}$$

$$F_x = \frac{E_1 E_2}{E_2 \cos^2\theta\left(\cos^2\theta + \left(\frac{E_1}{G_{12}} - 2v_{12}\right)\sin^2\theta\right) + E_1 \sin^4\theta} \times \varepsilon_x \eta_L A_f \cos\theta \tag{24}$$

Considering a rectangular specimen with dimensions a_1, a_2, and a_3 (Fig. 3), the amount of the short-fibers with length L and orientation θ, can be calculated as:

$$N = \frac{a_1 a_2 a_3 V_f f(l) g(\theta)}{A_f \bar{L}} = \frac{a_1 a_2 a_3 V_f f(l) g(\theta)}{A_f \bar{L}} \tag{25}$$

Then the number of fibers in the length of L and orientation of θ that cross the cross-section is:

$$N = \frac{a_1 a_2 a_3 V_f f(l) g(\theta)}{A_f \bar{L}} \times \frac{L\cos\theta}{a_1} = \frac{a_2 a_3 V_f f(l) g(\theta) L \cos\theta}{A_f \bar{L}} \tag{26}$$

The total applied forced applied to fibers in x direction on each layer can be formulated as:

$$F_x = \frac{a_2 a_3 V_f f(l) g(\theta) L\cos\theta}{A_f \bar{L}} \times \frac{E_1 E_2}{E_2 \cos^2\theta\left(\cos^2\theta + \left(\frac{E_1}{G_{12}} - 2v_{12}\right)\sin^2\theta\right) + E_1 \sin^4\theta} \times \varepsilon_x \eta_L A_f \cos\theta \tag{27}$$

Then the total force sustained by fiber in x direction for whole specimen can be calculated by:

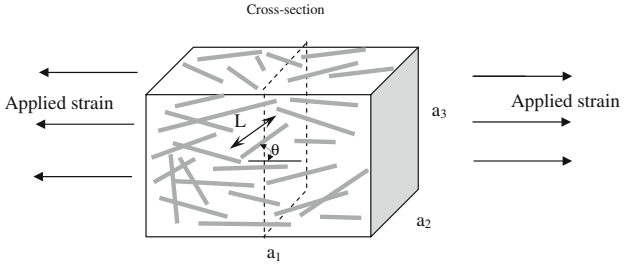

Fig. 3 The specimen of SWNTs/polymer composite

$$F_{\text{fibers}} = \int_0^{\pi/2}\int_{L_{\min}}^{L_{\max}} \frac{a_2 a_3 V_f f(l) g(\theta) L\cos\theta}{A_f \bar{L}} \times \frac{E_1 E_2}{E_2 \cos^2\theta\left(\cos^2\theta + \left(\frac{E_1}{G_{12}} - 2v_{12}\right)\sin^2\theta\right) + E_1 \sin^4\theta} \times \varepsilon_x \eta_L A_f \cos\theta \, dL \, d\theta \tag{28}$$

$$F_{\text{fibers}} = \frac{a_2 a_3 E_1 \varepsilon_x V_f}{\bar{L}} \int_{L_{\min}}^{L_{\max}} \eta_L L f(l) dL \int_0^{\pi/2} \frac{g(\theta)\cos^2\theta}{\cos^2\theta\left(\cos^2\theta + \left(\frac{E_1}{G_{12}} - 2v_{12}\right)\sin^2\theta\right) + \frac{E_1}{E_2}\sin^4\theta} d\theta \tag{29}$$

The whole force sustained by composite specimen can be calculated as:

$$F_{\text{composite}} = F_{\text{fibers}} + F_{\text{resins}} \tag{30}$$

$$F_{\text{composite}} = \frac{a_2 a_3 E_1 \varepsilon_0 V_f}{\bar{L}} \int_{L_{\min}}^{L_{\max}} \eta_L L f(l) dL \frac{E_2 \cos^2\theta g(\theta)}{E_2 \cos^2\theta\left(\cos^2\theta + \left(\frac{E_1}{G_{12}} - 2v_{12}\right)\sin^2\theta\right) + E_1 \sin^4\theta} d\theta + (1 - V_f) E_m \varepsilon_m \times a_2 a_3 \tag{31}$$

$$E_{\text{com}} = \frac{E_1 V_f}{\bar{L}} \int_{L_{\min}}^{L_{\max}} \eta_L L f(l) dL \int_0^{\pi/2} \frac{E_2 \cos^2\theta g(\theta)}{E_2 \cos^2\theta\left(\cos^2\theta + \left(\frac{E_1}{G_{12}} - 2v_{12}\right)\sin^2\theta\right) + E_1 \sin^4\theta} d\theta + (1 - V_f) E_m \tag{32}$$

Let

$$\lambda_s = \frac{1}{L}\int \left(1 - \frac{\tanh(\beta L/2)}{\beta L/2}\right) L f(L) dL \tag{33}$$

$$\lambda_O = \int_0^{\pi/2} \frac{g(\theta)\cos^2\theta}{\cos^2\theta(\cos^2\theta + m\sin^2\theta) + n\sin^4\theta} d\theta \tag{34}$$

where

$$m = \frac{E_1}{G_{12}} - 2v_{12} \tag{35}$$

$$n = \frac{E_1}{E_2} \tag{36}$$

The modified Cox model was achieved by substituting Eqs. 33 and 34 into Eq. 32:

$$E_{\text{com}} = \lambda_s \lambda_o E_f V_f + E_m(1 - V_f) \tag{37}$$

In the previous experiments, we have measured length distribution of carbon nanotubes through atomic force microscopy (AFM). The measured length was used for the Probability-Plot and it indicated that the length distribution can be represented with Weibull distribution, as shown in Fig. 4. This result was further confirmed by Chi-square goodness-of-fit test [35].

Therefore, the length of carbon nanotubes can be described by formation (38)

$$F(l) = \int_0^1 f(x)\mathrm{d}x = \int_0^1 abx^{b-1}\mathrm{e}^{-ax^b}\mathrm{d}x = 1 - \exp(-al^b) \tag{38}$$

while $\int_0^\infty f(x)\mathrm{d}x = \int_0^\infty abx^{b-1}\mathrm{e}^{-ax^b}\mathrm{d}x = 1$, a, b are the scale parameter and shape parameter, respectively.

Hence, the size-dependent shape factor can be computed as follows:

$$\begin{aligned}\lambda_s &= \frac{1}{l_{\text{mean}}}\int_{l_{\min}}^{l_{\max}} \left[1 - \frac{\tanh(\beta l/2)}{\beta l/2}\right] f(l) l \mathrm{d}l \\ &= \frac{1}{l_{\text{mean}}}\int_{l_{\min}}^{l_{\max}} \left[1 - \frac{\tanh(\beta l/2)}{\beta l/2}\right] abl^b \exp(-al^b)\mathrm{d}l\end{aligned} \tag{39}$$

For aligned short-fiber composite, Kacir et al. [36] propose the orientation can be approximated with a single parameter exponent distribution. This assumption is well matched with experiment results of the injection molding and twin-screw extrusion. So the orientation factor can be formulated as following:

$$g(\theta) = k\exp(-k\theta) \tag{40}$$

$$\lambda_O = \int_0^{\pi/2} \frac{k\exp(-k\theta)\cos^2\theta}{\cos^2\theta(\cos^2\theta + m\sin^2\theta) + n\sin^4\theta}\mathrm{d}\theta \tag{41}$$

For a hexagonal fiber packing arrangement, the following relationship exists [12]:

$$\frac{r}{R} = \left(\frac{\sqrt{3}V_f}{2\pi}\right)^{1/2} \tag{42}$$

R and r denote the fiber radius and the matrix radius of cylindrical shell encasing a concentric fiber, respectively. V_f denotes the volume percentage of carbon nanotubes.

Results and discussions

According to Eqs. 32–34, the elastic modulus of carbon nanotubes-reinforced polymer composite is dependent on the tube length distribution, tube dispersion, and tube orientation distribution. Epoxy polymer composites were taken as an example to analyze the effect of dispersion and orientation on nanocomposite modulus. The following data were used for the computation: $E_1 = 640$ GPa, $E_2 = 15$ GPa, $E_m = 2.5$ GPa [5]. The shear modulus of tube rope was changed as a function of rope diameters according to the experimental measurement [37], as shown in Fig. 5.

Orientation factor and shape factor were shown as functions of alignment angle, rope diameter, and length of the SWNTs (Fig. 6). Orientation factor increased with the decrease of alignment angle. When alignment angle was close to zero (zero means SWNTs are perfect aligned), the orientation factor was approximated to one. Small-diameter SWNTs seemed to be more sensitive to the orientation change. A slight improvement in the alignment led to a dramatic enhancement of orientation factor in the small-diameter SWNT ropes than in large-diameter ropes. Similarly, shape factor increased as rope diameter reduces.

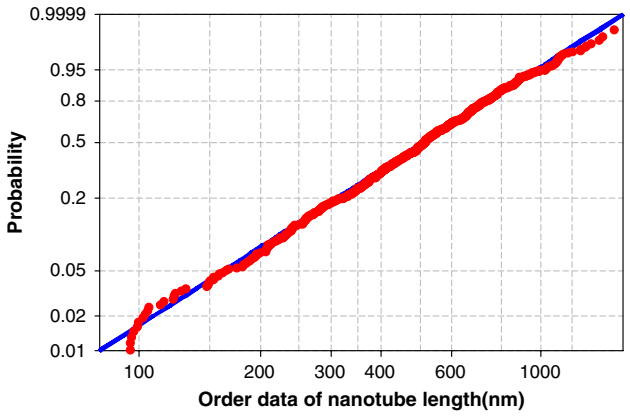

Fig. 4 Weibull probability plot for the distribution of carbon nanotube lengths

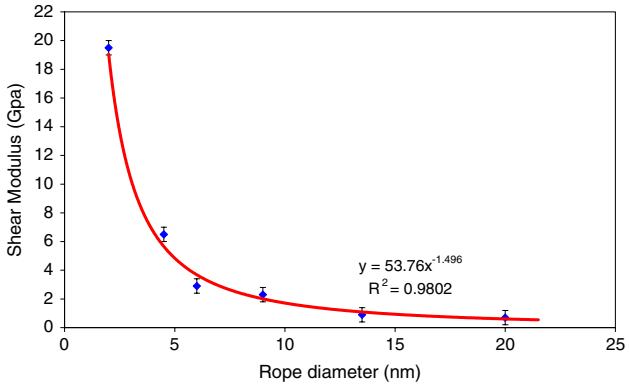

Fig. 5 Effect of rope diameter on the rope shear modulus

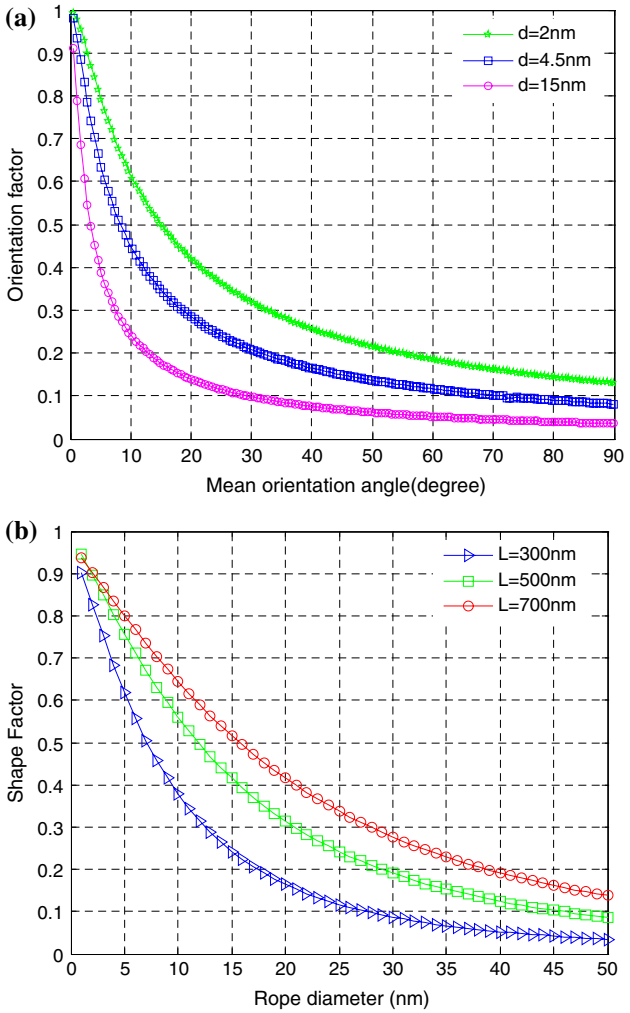

Fig. 6 (**a**) Orientation factor versus mean orientation angle at mean length $L = 500$ nm. (**b**) Shape factor versus rope diameter at 30% tube loading by volume

Variance of the rope length also had a significant effect on the shape factor. Even in the same dispersion condition, long SWNT rope showed a much higher shape factor than short one. Hence, long SWNTs were desired in the nanocomposite application due to the expected large contribution to the mechanical properties.

The elastic modulus of nanocomposite was predicted based on the modified rule of mixture (Eq. 37). Since orientation factor was a function of orientation angle and shape factor was a function of rope diameter, elastic modulus was a function of both orientation angle and rope diameter. The effects of SWNT dispersion and orientation on modulus are shown in Fig. 7. Obviously, in the zone of small diameter and low orientation angle, elastic modulus of nanocomposite showed a large value. With 30 wt% tube loading, well-dispersed and well-aligned SWNT composite displayed a modulus as high as 175 GPa. This was about

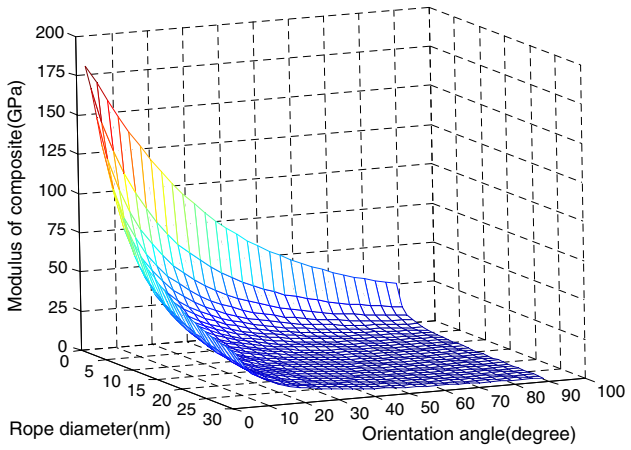

Fig. 7 Effect of rope diameter and orientation on the composite modulus

ten times modulus of glass fiber composite. In the zone of large diameter and large orientation angle, the graph surface of elastic modulus was almost flat. An improvement of alignment for large-diameter rope would not lead to a significant enhancement in the modulus. Similarly, an improvement of dispersion for large orientation would not achieve a considerable change in the composite modulus. As shown in Fig. 7, the nanocomposite modulus was increased when rope diameter was diminished or orientation-angle was reduced. Especially for small-diameter ropes, a minor change of orientation would result in a dramatic change in the modulus. Similar to the ropes with small orientation angle, a slight modification of the rope diameters resulted in substantial transformation in the modulus. Therefore, small diameter ropes had much more contribution to the modulus than large-diameter ropes, and their contribution was very sensitive to the orientation. Similarly, small-orientation-angle SWNT ropes had much more contribution than large-orientation-angle ones, their contribution was also very sensitive to the dispersion results.

By projecting the 3D surface of modulus to the modulus-orientation plane or modulus-rope diameter plane, the effect of dispersion and alignment could be seen more clearly. Figure 8a showed modulus of composite changes as a function of orientation angle. When mean orientation angle was getting less than 20°, a slight decrease in the orientation angle would lead to a dramatic enhancement. The smaller the rope diameter, the larger magnitude the modulus changed. Elastic modulus, as function of rope diameter, was shown in the Fig. 9a. The well-aligned SWNT composite would lead to a considerable change of modulus due to slight modification of the rope diameters. The effects of tube loading were also plotted in Figs. 8b and 9b. Obviously, well-aligned or well-dispersed SWNT composites showed high growth coefficient with increasing tube loading.

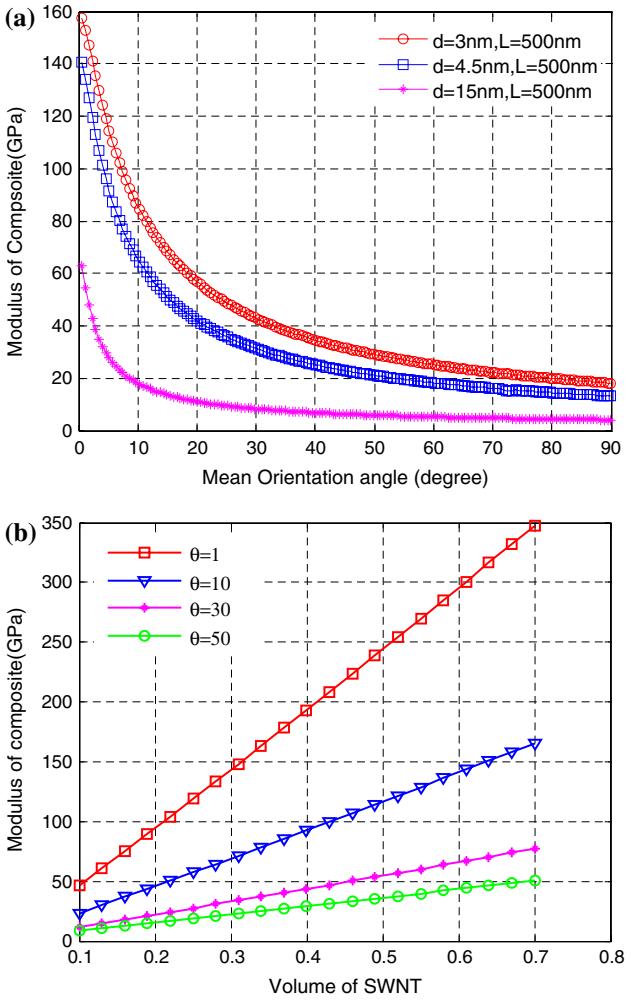

Fig. 8 (**a**) Composite modulus versus mean orientation angle at mean length $L = 500$ nm. (**b**) Composite modulus versus tube loading by volume at rope diameter d = 4.5 nm, $L = 500$ nm

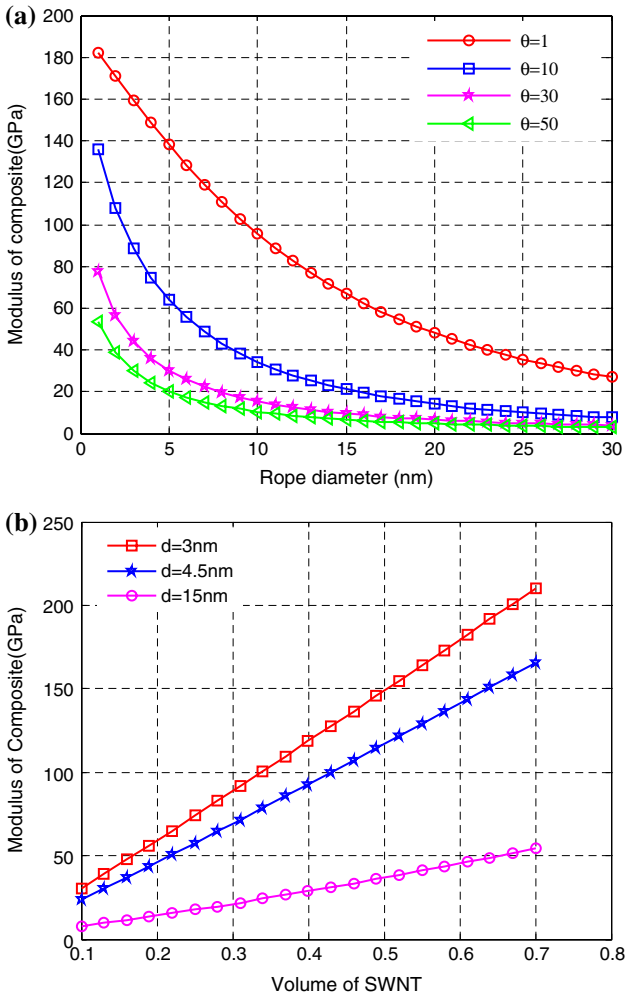

Fig. 9 (**a**) Composite modulus versus rope diameter at mean length $L = 500$ nm. (**b**) Composite modulus versus tube loading by volume at rope diameter $\theta = 10°$, $L = 500$ nm

The computational results were also compared with experimental measurements. Shankar [38] achieved aligned single-walled carbon nanotubes film under strong magnetic field. The aligned SWNTs were further used to fabricate epoxy nanocomposites. With a loading of ~56%, the measured storage modulus is around 47 GPa. The average diameter of dispersed SWNTs is ~4.5 nm and average orientation is 39°. According to the above calculation, the prediction of modulus is 56 GPa. Therefore, the computation result is consistent with the experimental outcome.

Comparing the experimental and calculated results, there is about 19% deviation. Interfacial bonding may be an important explanation. In our modeling, a perfect interfacial bonding is assumed, but it is very difficult for nanocomposites to achieve perfect interface. Load-transfer capacity may significantly compromise the expected enhancement. Another possible reason may come from the modulus prediction of nanotube ropes. Nanotube ropes are composed of individual nanotubes, which are not in the same length. Hence, nanotube ropes may not have uniform diameters across the axis. In the theoretical calculation, all the nanotube ropes are assumed to have uniform diameter and accordingly generate some errors. In addition, the orientation angle may not exactly follow the exponential distribution. Assuming alignment follows exponential distribution may also lead to some errors. Even though these kinds of issues affect the precision of the predictions, the deviation is still in the range of acceptance.

Due to the extraordinary properties of carbon nanotubes, they are actively being investigated for the composite applications. Accurate models of how nanotube orientation and dispersion influence the effective properties of the SWNTs-reinforced polymer is necessary to optimize the fabrication and effective properties of SWNT polymer systems. In particular, modeling of effective behavior for

SWNTs-reinforced composite is complicated by the range of length scales characteristic of these materials. This modified Cox model innovatively uses statistical theory to address the effect of nanotubes morphology (diameter and length) and alignments, and provides an acceptable prediction on the composite modulus. We believe the proposed modeling will provide valuable guidance for nanocomposites manufacturing to realize their potential as lightweight strong materials.

Conclusions

A modified Cox model was established to predict the elastic modulus of SWNTs/polymer composite. The effects of dispersion and orientation were thoroughly discussed. The computational results indicated elastic modulus of nanocomposite was maximized in the zone of small diameter and low orientation angle. Small-diameter ropes had much more contribution to the modulus than large-diameter ropes, and their contribution was very susceptible to the orientation. Similarly, SWNT ropes with small orientation angle had much more contribution than those with large-orientation-angle, and their contribution was correspondingly very sensitive to the dispersion results. The modeling and computational analysis provided in-depth understanding on carbon nanotube/polymer systems and will present valuable guidance to optimize the composite fabrications for high performance.

References

1. Wong EW, Sheehan PE, Lieber CM (1997) Science 277:1971. doi:10.1126/science.277.5334.1971
2. Bernholc J, Brenner D, Buongiorno Nardelli M, Meunier V, Roland C (2002) Annu Rev Mater Res 32:347. doi:10.1146/annurev.matsci.32.112601.134925
3. Dujardin E, Webbesen TW, Krishan A, Yianilos PN, Trecy MMJ (1998) Phys Rev B 58:14013. doi:10.1103/PhysRevB.58.14013
4. Lu J (1997) Phys Rev Lett 79:1297–1299. doi:10.1103/PhysRevLett.79.1297
5. Liu T, Kumar S (2003) Nano Lett 3:647. doi:10.1021/nl034071i
6. Kong J, Soh HT, Cassell AM, Quate CF, Dai H (1998) Nature 395:878. doi:10.1038/27632
7. Yu MF, Files BS, Arepalli S, Ruoff RS (2000) Phys Rev Lett 84:5552. doi:10.1103/PhysRevLett.84.5552
8. Belytschko T, Xiao SP, Schatz GC, Ruoff RS (2002) Phys Rev B 65:235430. doi:10.1103/PhysRevB.65.235430
9. Walters DA, Ericson LM, Casavant MJ, Liu J, Colbert DT, Smith KA et al (1999) Appl Phys Lett 74:3803. doi:10.1063/1.124185
10. Saito R, Fujita M, Dresselhaus G, Dresselhaus MS (1992) Appl Phys Lett 60:2204. doi:10.1063/1.107080
11. Dresselhaus MS, Dresselhaus G, Avouris P (2001) Carbon nanotubes: synthesis, structure, properties and applications, 1st edn. Springer Verlag, New York
12. Budiansky B (1965) J Mech Phys Solids 13:223. doi:10.1016/0022-5096(65)90011-6
13. Chow TS (1977) J Appl Phys 48:4072. doi:10.1063/1.323432
14. Russel WB (1973) Z Angew Math Phys 24:581. doi:10.1007/BF01588160
15. Chou T-W, Nomura S, Taya M (1980) J Compos Mater 14:178. doi:10.1177/002199838001400301
16. Hashin Z (1968) J Compos Mater 2:284. doi:10.1177/002199836800200302
17. Laws N, McLaughlin R (1979) J Mech Phys Solids 27:1. doi:10.1016/0022-5096(79)90007-3
18. Benveniste Y (1987) Mech Mater 6:147. doi:10.1016/0167-6636(87)90005-6
19. Chen C-H, Cheng C-H (1996) Int J Solids Struct 33:2519. doi:10.1016/0020-7683(95)00278-2
20. Chow TS (1978) J Polym Sci Polym Phys 16:959. doi:10.1002/pol.1978.180160602
21. Mori T, Tanaka K (1973) Acta Metall 21:571–574. doi:10.1016/0001-6160(73)90064-3
22. Halpin JC (1969) J Compos Mater 3:732
23. Halpin JC, Kardos JL (1976) Polym Eng Sci 16:344. doi:10.1002/pen.760160512
24. Thostenson ET, Chou T-W (2003) J Phys D Appl Phys 36:573. doi:10.1088/0022-3727/36/5/323
25. Ashrafi B, Hubert P (2006) Comp Sci Tech 66:387. doi:10.1016/j.compscitech.2005.07.020
26. Jiang B, Liu C, Zhang C, Wang B, Wang Z (2007) Compos Part B 38:24. doi:10.1016/j.compositesb.2006.05.002
27. Cox HL (1952) Br J Appl Phys 3:72. doi:10.1088/0508-3443/3/3/302
28. Nayfeh AH (1977) Fibre Sci Tech 10:195. doi:10.1016/0015-0568(77)90020-3
29. McCartney LN (1992) Analytical models of stress transfer in unidirectional composites and cross-ply laminates, and their application to the prediction of matrix/transverse cracking. Proceedings of IUTAM Symposium, Blacksburg, VA, 1991, 251
30. Nairn JA (1973) Mech Mater 26:63. doi:10.1016/S0167-6636(97)00023-9
31. Fukuda H, Kawata K (1974) Fiber Sci Tech 7:207. doi:10.1016/0015-0568(74)90018-9
32. Jayaraman K, Kortschot MT (1996) J Mater Sci 31:2059. doi:10.1007/BF00356627
33. Kallmes O, Bernire G, Perez MA (1977) Pap Tech Ind 18:222
34. Fu SY, Lauke B (1998) Comp Sci Tech 58:389
35. Wang S, Liang Z, Wang B, Zhang C (2006) Nanotechnology 17:634. doi:10.1088/0957-4484/17/3/003
36. Kacir L, Narkis M, Ishai O (1975) Polym Eng Sci 15:525. doi:10.1002/pen.760150708
37. Salvetat JP, Andrew G, Briggs D, Bonard JM, Bacsa RR, Kulik AJ, Stöckli T, Burnham NA, Forró L (1999) Phys Rev Lett 82:944. doi:10.1103/PhysRevLett.82.944
38. Shankar KR (2003) Department of Industrial Engineering, Master of Science thesis, Preparation and characterization of magnetically aligned carbon nanotubes buckypaper and composites